International Journal for Housing Science and Its Applications
Publish August 10, 2025. Volume 46, Issue 4 Pages 2676-2694

https://doi.org/10.70517/ijhsa464224

Design Innovation and Application Demonstration of New Photovoltaic Building Integration Perimeter Protection Systems in the Low-Carbon Economy Era

Jian Huang[1], Fazhi Wang[1], Dongyao Wang[1], Shihao Liu[1,*], Pizhuang Wang[1], Lili Xiao[1] and Beibei Chen[1]
[1] R&D Center, FAR EAST FACADE (Zhuhai) LIMITED., Zhuhai, Guangdong, 519090, China
Corresponding authors: (e-mail: ln1278518520@163.com).

Abstract New photovoltaic building integration is the integration of photovoltaic components into building envelope structures. It is an efficient building envelope energy-saving technology that greatly expands the utilization potential of photovoltaic components, promotes the development of building energy-saving technologies, and contributes to the achievement of the “dual carbon” goals. From an architect's perspective, this paper integrates architecture, technology, and aesthetics to propose a new photovoltaic building integration envelope system. The thermal-electric performance and daylighting performance of BIPV copper indium gallium selenide photovoltaic ventilation windows were investigated. Using sensitivity indices as quantitative metrics, the sensitivity of thermal-electric output indicators of exterior envelope systems in representative cities across different climate zones to changes in specific design parameters was analyzed, providing technical priorities and scientific guidance for the design of BIPV exterior envelope systems in various climate zones. Based on experimental simulation results, the copper indium gallium selenide photovoltaic ventilation window components exhibit high current conversion per unit area, high output power, superior high-temperature and high-pressure resistance, and an effective daylighting rate of 76.43%. The new BIPV exterior envelope system can simultaneously meet the thermal requirements of buildings in different seasons or climates. By utilizing the residual heat from photovoltaic glass to drive airflow through channels, passive cooling or heating can be achieved, enabling the comprehensive utilization of solar photovoltaic and thermal energy on the exterior window surfaces of buildings.

Index Terms BIPV; exterior envelope system; sensitivity analysis; copper indium gallium selenide (CIGS)

I. Introduction

The world's energy consumption has surged dramatically, and the ecological environment has continued to deteriorate, particularly due to greenhouse gas emissions, which have led to increasingly severe global climate change. This has posed a serious threat to the sustainable development of human society, and addressing climate change has become a major challenge faced by the global community [1]-[4]. Against the backdrop of global warming attracting the attention of governments worldwide, the concept of a low-carbon economy has emerged [5]. A low-carbon economy is a new model of economic development that emphasizes achieving greater economic output with fewer greenhouse gas emissions, holding profound strategic significance for the world's development [6]-[8]. Against this backdrop, the design innovation and application of new photovoltaic building-integrated envelope systems have become important initiatives in the era of a low-carbon economy [9], [10].

PV-BIMB systems integrate solar photovoltaic arrays into a building's envelope structures (such as roofs and walls) or building components (such as sunshades and skylights), closely integrating them with building functions to achieve an integrated system of building and photovoltaic power generation [11]-[14]. It is not simply about attaching photovoltaic power generation devices to buildings, but rather considering the integration of photovoltaic power generation systems throughout the entire process from building design, construction, to use, making it an organic component of the building as a whole [15]-[18]. Photovoltaic building-integrated envelope systems can utilize solar energy to convert light energy into electricity, providing power for the building itself and surrounding areas, significantly reducing the building's reliance on the traditional power grid and lowering electricity costs [19]-[21]. Photovoltaic power generation is a clean energy source that does not produce greenhouse gas emissions during the power generation process [22]. Compared to traditional thermal power generation, the electricity generated by photovoltaic building-integrated envelope systems can effectively reduce emissions of pollutants such as carbon dioxide and sulfur dioxide [23]-[25]. Additionally, photovoltaic building-integrated envelope systems can seamlessly blend with the building's exterior, becoming an integral part of the architectural design [26], [27].

Literature [28] discusses the development of solar photovoltaic technology in building integration and design, pointing out that PV-BIM systems are a powerful tool for achieving the growing demand for zero-energy buildings, and introduces the challenges they face as well as their advantages in terms of value and aesthetics. Literature [29] aims to develop a parametric research method to determine the balance between floor area and the required PV-BIM area in form-following envelope structures to meet energy demands. The study results indicate that the sufficiency of generated energy is influenced by its form and orientation. Literature [30] reviews the barriers and risks associated with the application of photovoltaic building-integrated (BIPV) systems and analyzes solutions. The results indicate that the greatest barriers to BIPV systems are tariffs and public acceptance, emphasizing the slow progress of their practical application. Literature [31] provides an overview of BIPV system operation, usage benefits, and performance improvement technologies, aiming to offer new users and researchers the latest information on BIPV systems. Literature [32] proposes the use of semi-transparent BIPV systems on the vertical sections of building facades to achieve on-site clean energy generation, compares BIPV with existing photovoltaic modules, and introduces the environmental sustainability of BIPV systems in buildings. Literature [33] examines the development, implementation, and barriers to widespread adoption of BIPV. It emphasizes the advantages of BIPV technology, including cost reduction, aesthetic appeal, and reliability, while also highlighting barriers such as lack of awareness and expertise. Literature [34] proposes an economic analysis method for BIPV, aiming to quantify the social and environmental advantages of BIPV systems and incorporate these values into economic analysis. The study verifies the economic feasibility of replacing traditional building materials with BIPV systems. Literature [35] reviews BIPV technology, including the main developments of various BIPV systems, the impact of experimental base systems on building performance, and the development, application, and current status of BIPV systems, identifying research needs and opportunities.

Literature [36] discusses the annual performance and economic feasibility of grid-connected building-integrated photovoltaic (GBIPV) systems under India's hot and humid climate conditions, revealing the numerous advantages and challenges associated with the application of GBIPV systems in building structures. Literature [37] systematically evaluates research on BIPV technology in net-zero energy buildings (NZEB) and emphasizes the importance of factors such as window-to-wall ratio in achieving NZEB standards through case analysis. Literature [38] points out that artificial central air conditioning systems are widely used in large buildings, emphasizing that such buildings consume a significant amount of energy and face issues such as poor indoor air circulation and low cooling system efficiency. Therefore, it proposes BIPV systems to address these issues. Literature [39] reviews the primary energy characteristics of BIPV systems, aiming to provide references for researchers, architects, and BIPV manufacturers, and systematically introduces the relevant performance of BIPV systems to promote their continued development and inform appropriate standardization efforts. Literature [40] indicates that utilizing BIPV systems as building materials to design renovation strategies is an important method to achieve the decarbonization of building stock in an economical and environmentally friendly manner, and emphasizes the economic and environmental benefits of BIPV in building renovations.

This paper integrates photovoltaic building materials into building envelopes or structural components without compromising the power generation performance of photovoltaic modules, ensuring building safety while fulfilling the functions of building envelopes. The paper applies copper indium gallium selenide (CIGS) thin-film photovoltaic materials with semi-transparency and high conversion efficiency to building windows to enhance power generation efficiency and improve indoor lighting conditions. The electrical performance of BIPV cell modules under different irradiation conditions and the impact of BIPV systems on indoor thermal environments were investigated. Additionally, using light transmission rate (UDI) and discomfort glare index (DGI) as evaluation metrics, the indoor illuminance and glare performance of copper indium gallium selenide photovoltaic ventilation windows were studied. Key parameters include photovoltaic curtain wall height, airflow channel spacing, and building exterior wall thermal conductivity coefficient. System thermal-electric output metrics include annual total electricity generation per unit photovoltaic curtain wall area, annual total airflow channel heat generation, and annual total indoor heat transfer. Sensitivity analysis of thermal-electric output for BIPV envelope systems in representative cities across climate zones was conducted using sensitivity indices as quantitative metrics. Finally, simulations were conducted on the tilt angles of photovoltaic modules installed on building roofs and facades in different seasons. By comparing with actual data, the optimal installation tilt angle for photovoltaic modules in buildings was proposed, fully considering the installation area and economic benefits of photovoltaic modules, providing theoretical reference for the design of building envelope structures in photovoltaic building integration systems.

II. Design of BIPV Perimeter Enclosure Systems

II. A. Design Content

The preliminary design of a BIPV system is based on architectural functionality. When designing a BIPV system, the principles of architectural functionality and aesthetics should be considered first. Based on climate data of the building's location, architectural design style, characteristics of the building's envelope structure, and surrounding environment, the installation location and form of photovoltaic components for the BIPV system should be determined. When determining the installation location of the BIPV system, it is important to avoid or stay away from shading objects and select the optimal orientation and tilt angle for the solar panels. Once the location and form of the BIPV system are determined, the type and area of the photovoltaic components can be finalized. At this stage, the installation location, form, type, and power of the photovoltaic components in the BIPV system can be basically determined.

Traditional photovoltaic modules often give the impression of being bulky and monotonous, making it difficult to harmoniously integrate with the overall appearance of the building. While large-sized, single-color photovoltaic modules can perform power generation functions, they may negatively impact the aesthetic appeal of the building, even giving a rigid or jarring impression. However, the BIPV modules adopted in this project perfectly address this issue. These BIPV modules not only have excellent power generation performance, converting solar energy into electricity, but also achieve a seamless integration with the building's exterior through clever design, creating a unique architectural aesthetic effect. The photovoltaic curtain wall features a semi-transparent design, complementing the building's glass curtain wall. The semi-transparent photovoltaic modules absorb solar energy while allowing a certain amount of natural light to pass through, meeting lighting requirements while creating a unique play of light and shadow inside the building. This transparent and dynamic design aligns perfectly with the modern architectural philosophy of simplicity, openness, and transparency, fully showcasing the technological and fashionable aspects of modern architecture. In addition to harmoniously integrating with the building's exterior, the BIPV system in this project also adds a vibrant touch of color to the building through diverse component forms and color options [41].

II. B. Wall modules

The basic structural units of wall modules in BIPV exterior envelope systems are primarily divided into three layers: the main structural framework, photovoltaic panels bonded to the outer side, and composite insulation panels installed on the inner side. The dimensions of the four types of wall modules—basic facade, corner, door, and window—are coordinated and organized based on the standard module size of 500mm × 1100mm photovoltaic panels. At the basic design level of wall panel modules, key factors include the treatment of panel joints between photovoltaic panels, the joint treatment of door and window components, the integration of the skeleton support frame with the outer photovoltaic panels and inner composite materials, and the connection and construction of wall panel modules with the structural main frame columns, beams, and girders. These elements are critical to forming an integrated enclosure interface. Detailed node construction designs are explored in the following section.

II. C. Roof panel module

The roof panels of the BIPV experimental building are constructed in a manner similar to the wall panels, consisting of several identical modular units. However, unlike the wall panels, the roof panels must not only provide energy-saving benefits but also bear additional load weights. Therefore, there are differences in the selection of structural materials and construction methods between the two. The entire structure is supported by a steel framework connected to the main structural beams. It can be primarily divided into two identical roof module assemblies. Each module forms a 700mm-wide convex skylight space through variations in the steel framework support. The upper part of the skylight is further equipped with adjustable-angle support steel frames to install three adjustable-angle thin-film photovoltaic modules measuring 500mm × 1100mm. The roof panels can dynamically adjust the angle of the photovoltaic modules to maximize solar radiation reception, thereby enhancing the photovoltaic conversion efficiency of the roof modules and improving the building's overall energy-saving benefits. Heat-collecting air pipes and heat treatment devices are installed above the roof panels. The heat-collecting pipes are connected to the heat intake ports at the top of the wall panel modules. When the cavity temperature reaches a certain level, mechanical ventilation is used to recover the hot air from the cavity. This air is then processed through an air-source heat pump to achieve heat recovery and thermal energy conversion. When the cavity temperature is at a lower level, the heat collection pipes and heat pump system are not used. In summer, natural ventilation formed by temperature differences is utilized to lower the cavity temperature, while in winter, the sealed cavity achieves thermal insulation for the facade.

II. D.Floor panels

Floor slabs are an indispensable component of the building envelope, essential for achieving structural integrity. In building projects where a steel frame system serves as the primary structural framework, floor slab system design strategies and construction techniques vary widely, including prefabricated removable reinforced steel truss slab systems, prefabricated non-removable reinforced steel truss slab systems, closed-end slab-YJ type profiled steel plate systems, and deep rib slab systems, among others. These floor slab systems each have their own advantages in terms of transportation, construction, cost, and architectural adaptability.

In this BIPV unit, floor slabs serve two primary functions and roles: electrical connection and internal insulation. In terms of electrical connection requirements, the electrical lines from the wall panel modules are routed along the vertical studs to the lower part of the cavity and connected to the pre-installed electrical outlets through the floor slab, thereby linking the facade module units to the building's main electrical system. Therefore, to facilitate connection, disassembly, inspection, and maintenance, the floor panels adopt a movable construction method. In terms of insulation requirements, the upper insulation layer of the floor panels connects with the composite insulation panels on the inner side of the wall panels, forming an integrated insulation interface.

II. E. Composition of photovoltaic systems

The composition of a photovoltaic power generation system is primarily divided into two parts: photovoltaic conversion cell modules and power supply generation equipment. These can be further categorized into photovoltaic panels, solar cells, controllers, inverters, batteries, and other accessories.

Photovoltaic conversion cell modules, also known as photovoltaic devices, are components that convert solar energy into electrical energy and serve as the core of the photovoltaic system. Solar cells are the components that make up these modules. Each cell is sandwiched between front and back pressure plates, with the outer layer typically made of low-iron glass and the inner layer lined with additional materials, forming a complete photovoltaic module unit. The materials used to manufacture these cells are listed in Table 1, including monocrystalline silicon, polycrystalline silicon substrate-based cells, compound semiconductor thin-film cells, and emerging battery materials such as dye-sensitized solar cells.

Table 1: Classification of the material of photovoltaic cells

Material	Form	Merit	Shortcoming
Crystal silicon (single crystal silicon c-si-polysilicon p-si)	Plate type	The size, module and thickness of crystalline silicon photovoltaic components can meet the demand of the structure	There is a clear circuit line between the battery films and the poor color
Compound semiconductor film battery (Selenium gallium copper CIGS)	Film type	The whole life cycle has more power generation, weak light sex, low attenuation rate, small temperature influence and stable performance. Meet the demand of architectural aesthetics, the color and texture are rich	The unit area power and component conversion efficiency are slightly lower than the silicon components
Compound semiconductor film battery (cadmium telluride CdTe)	Film type	The characteristics of low temperature coefficient, low performance, high stability and small effect of hot spot effect are suitable for the use of high quality buildings	The unit area power and component conversion efficiency are lower than the silicon components. The price is higher. Cadmium as a heavy metal is toxic and can cause pollution
Dye photochemical cell	New form	It is composed of dye sensitizer, oxidizing reductant electrolyte, nano-porous semiconductor film, electrode and conductive basis	Solid dye-sensitized batteries are only half as efficient as liquid batteries

Among various photovoltaic conversion cell components, the photovoltaic material used in the curtain wall of the BIPV system studied in this paper is copper indium gallium selenide (CIGS). CIGS is a highly stable, high-performance, and relatively mature thin-film photovoltaic technology. Since 1986, CIGS thin-film photovoltaic technology has gradually emerged as a leading photovoltaic technology in the rapidly growing photovoltaic market, thanks to its visual advantages, environmental advantages, production advantages, and performance advantages.

II. F. System Monitoring

The primary components of BIPV system monitoring include real-time power generation monitoring, solar radiation intensity statistics, and environmental temperature monitoring. After commissioning and operation, the monitoring devices installed in the system will continuously record system load and power generation, serving as the most reliable evidence of the system's actual operational efficiency. Through deviation analysis, these data can also be used for theoretical power generation calculation formulas, parameter adjustment, and other tasks. Solar radiation

intensity and collector environmental temperature statistics are key focuses of BIPV system monitoring. Among these, the solar radiation intensity used in theoretical power generation calculations is based on typical meteorological annual data. Actual meteorological deviations can lead to errors in actual power generation. According to statistics, for every 1°C increase in collector environmental temperature, the peak power loss rate of photovoltaic cells is approximately 0.32–0.43%. This results in a reduction in the photovoltaic system's cell array photovoltaic conversion efficiency under high-temperature operating conditions, ultimately affecting the system's actual power generation.

III. Experimental simulation process

The simulation tools used in this paper include the building energy consumption simulation software EnergyPlus, the building drawing software SketchUp, and the OpenStudio software. The overall simulation approach in this paper is as follows: use SketchUp software to create a physical model of the building, and use OpenStudio software to assign thermal properties to this physical model. In EnergyPlus software, set the parameters for building energy consumption simulation, and establish a numerical simulation model for photovoltaic building heat transfer and power generation. Set the building envelope material information, schedule, ground temperature, indoor occupancy, lighting, building equipment, HVAC system, and other parameters required for energy consumption simulation. Set the simulation time step, run the IDF file, and output the simulation results for the power generation capacity of the photovoltaic modules and the surface temperature of the photovoltaic glass. Compare these results with experimentally measured data. Use the Mean Bias Error (MBE) and Root Mean Square Error Variation Coefficient (CVRMSE) parameters to compare the simulated values with the experimental values, verifying the accuracy of the simulation model and laying the foundation for subsequent simulation analysis work.

IV. Heat transfer and power generation test results for BIPV components

IV. A. Electrical Design of Photovoltaic Cell Modules

BIPV photovoltaic cell modules are formed by connecting individual solar cells in series and parallel configurations. The electrical performance of the module changes with the number of series and parallel connections of the individual cells, and its electrical performance parameters change accordingly. When solar cells are connected in series, the current of the cell array remains unchanged, and the voltages are added together. When cells are connected in parallel, the voltage of the cell array remains unchanged, and the currents are added together. The characteristics of BIPV photovoltaic cell modules are shown in Figure 1.

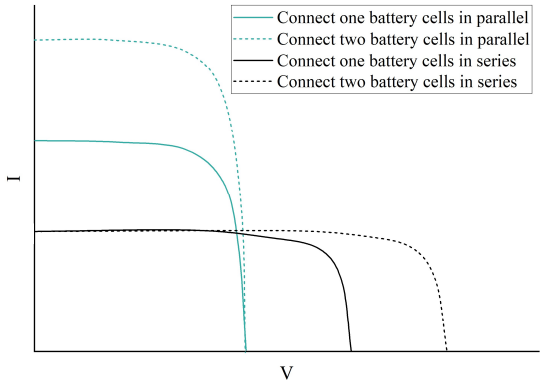

Figure 1: Series characteristics and parallel characteristics of the solar cells

When designing the output parameters of photovoltaic (PV) module assemblies, it is essential to consider the output characteristics of PV module assemblies as the smallest power-generating units within a PV power generation system, thereby enhancing their flexibility during application. Typically, factors such as the physical dimensions of the PV module assemblies, compatibility with battery banks operating at 12V or other integer multiples, and compatibility with the startup voltage and maximum input current of standard inverters must be taken into account. Particularly for innovative applications, it is crucial to align with current market conditions to swiftly capture market share. The promotion and application of photovoltaic cell technology also require consideration of adaptability and other issues. This chapter designs a circuit for photovoltaic cell modules that minimizes mismatch losses caused by inconsistent electrical performance on the back side of photovoltaic cells and is compatible with existing photovoltaic module production lines. Production can be initiated by simply adding a laser dicing machine and modifying the string welding machine.

After determining the circuit design principles mentioned above, the output characteristics and dimensions of the photovoltaic cell module are designed according to conventional photovoltaic module specifications, as shown in Table 2. The design aims to minimize modifications to accommodate the processing capabilities of existing photovoltaic module production lines.

Table 2: Conventional pv module specifications

Product type	60P	75P	60G	75G
Contour length (mm)	1638	1954	1657	1970
Contour width (mm)	981	981	981	981
Contour thickness (mm)	39	39	5	6
Product weight (mm)	18	21	24	28
Nominal power (W)	265	320	260	315
Working voltage V_m (V)	29	38	30	30
Working current I_m (A)	6.81	8.34	8.41	6.59
Open circuit voltage V_{oc} (V)	39	45	38	46
Short circuit current I_{sc} (A)	10.05	9.44	8.08	9.01
Rated battery working temperature (℃)	50±3.0	50±3.0	50±3.0	50±3.0
Maximum power temperature coefficient (%/℃)	-0.45	-0.45	-0.45	-0.45
Open circuit voltage temperature coefficient (%/℃)	-0.35	-0.35	-0.40	-0.40
Short circuit current temperature coefficient (%/℃)	0.08	0.08	0.10	0.10

Based on the specifications of photovoltaic cells in mass production, as shown in Table 3, design an ideal cutting plan for photovoltaic cells.

Table 3: Photovoltaic cell sheet specifications

Project	$V_m(V)$	$I_m(A)$	$V_{oc}(V)$	$I_{sc}(A)$	$P_m(W)$	$\mu(\%)$	$bifi(\%)$
Positive electrical performance parameters	0.59	9.50	0.65	9.81	5.00	20.5	86.24
Reverse electrical performance parameters	0.60	7.50	0.70	7.50	4.28	16.55	
Size	155mm×155mm±0.25mm						
Thickness	200μm±25μm						
Maximum power temperature coefficient	-0.40%/℃						
Open circuit voltage temperature coefficient	-0.35%/℃						
Short circuit current temperature coefficient	0.10%/℃						

Based on the open-circuit voltage range of the designed photovoltaic cell module, V_{oc} ranging from 38V to 48V, and the value of the photovoltaic cell V_{oc}, which is 0.65V, determine the number of cells in series, N. The expression is as follows:

$$N = \frac{V'_{oc}\beta}{V'_{oc}\beta'} \tag{1}$$

In the formula: β is the open-circuit voltage of the photovoltaic module. β' is the open-circuit voltage of the photovoltaic cell.

Based on the number of encapsulated cells, the 75G-type scheme can be selected; the 60G-type scheme is not recommended. The 75G-type scheme has minimal impact on the series-parallel design of the photovoltaic array. If photovoltaic module laminated encapsulation technology is applied, the scheme of cutting photovoltaic cells followed by series-parallel connection should be chosen to reduce power losses due to current mismatch on the back side of the photovoltaic cells. Photovoltaic cells can be equally divided and cut into areas ranging from 1/5 to 1/2 of their original size.

After cutting the photovoltaic cells, the IV characteristics of the cut photovoltaic cells are shown in Figure 2. It can be seen that the open-circuit voltage of the photovoltaic cells changes very little after cutting, while the short-circuit current decreases proportionally to the area of the cut photovoltaic cells.

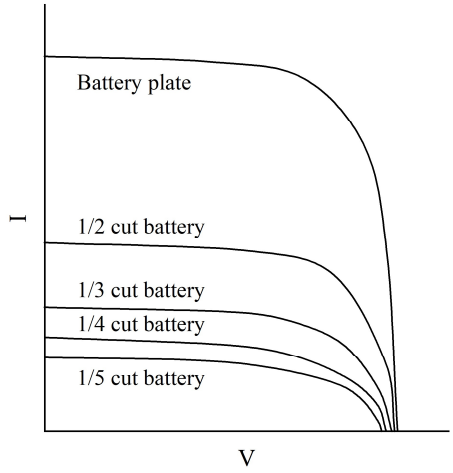

Figure 2: IV characteristics after solar cell cutting

The series-parallel design schemes for copper indium gallium selenide (CIGS) photovoltaic cells are shown in Table 4. The seven schemes listed in the table should be selected based on the actual circumstances of photovoltaic module manufacturing companies. If the optimal scheme is to be determined based on the objectives of product standardization and ease of large-scale production, Scheme 5 is recommended. Reasons:

(1) The number of photovoltaic cells to be cut is moderate and consistent with existing stacking cutting schemes, eliminating the need to redesign the main and auxiliary grid printing screens for photovoltaic cell electrodes.

(2) The series length of the photovoltaic cell series is moderate, reducing quality losses during the photovoltaic cell series arrangement process.

(3) The photovoltaic cell area ratio within the photovoltaic cell module is small, providing more space to arrange the electrical spacing within the module, thereby improving the yield rate of the encapsulation process.

(4) The external dimensions of the photovoltaic cell module are compatible with the production capacity of mainstream lamination equipment used by various companies, minimizing the impact on lamination process output.

(5) The external dimensions of the photovoltaic cell module still have room for expansion, allowing for the installation of frame brackets, junction boxes, and other accessories without obstructing the back of the photovoltaic cells, thereby avoiding any reduction in power generation on the back of the photovoltaic cell module.

Table 4: Series parallel design of photovoltaic cells

Scheme number	Cutting scheme	Series parallel design	Component size (mm)	Junction box position
Solution 1	Noncutting	72 series 1 parallel	2000×1000	Shoreline
Solution 2	1/2 cutting	9 series / 2 parallel / 8 series	1980×1100	By long side three
Solution 3	1/3 cutting	18 series / 3 parallel / 4 series	2000×990	Shoreline
Solution 4	1/4 cutting	36 series / 3 parallel / 2 series	1980×1050	In the middle
Solution 5	1/5 cutting	12 series / 5 parallel/ 6 series	1650×1000	In the middle
Solution 6	1/6 cutting	72 series/8 parallel	1900×990	Shoreline
Solution 7	1/7 cutting	18 series / 6 parallel / 4 series	1800×1100	In the middle

Through simulation modeling, the IV and P-V curves of copper indium gallium selenide photovoltaic cell modules under different illuminance levels were obtained, as shown in Figure 3. It can be seen that the advantages of copper indium gallium selenide cell modules are obvious: they convert more current per unit area and have higher output power. They also have stronger resistance to high temperatures and high-voltage-induced degradation.

IV. B. Heat Transfer and Power Generation Performance

This section analyzes the heat transfer and power generation performance of copper indium gallium selenide photovoltaic ventilation windows. Internal circulation experiments were conducted during the daytime on April 20, 2024, and external circulation experiments were conducted during the daytime on May 14, 2024. Figure 4 shows the meteorological data for these two days. It can be observed that the ambient temperature fluctuates with changes in solar radiation. During the internal circulation mode experiment, the incident radiation on the window surface reached 655 W/m² at noon, with the ambient temperature varying between 7°C and 16°C. By 14:00 in the afternoon, due to cloud cover, both radiation and temperature suddenly dropped. During the external circulation mode, the

maximum solar radiation was 539 W/m². The lowest environmental temperature was 18°C in the morning, and the highest was 32°C at 13:30 in the afternoon.

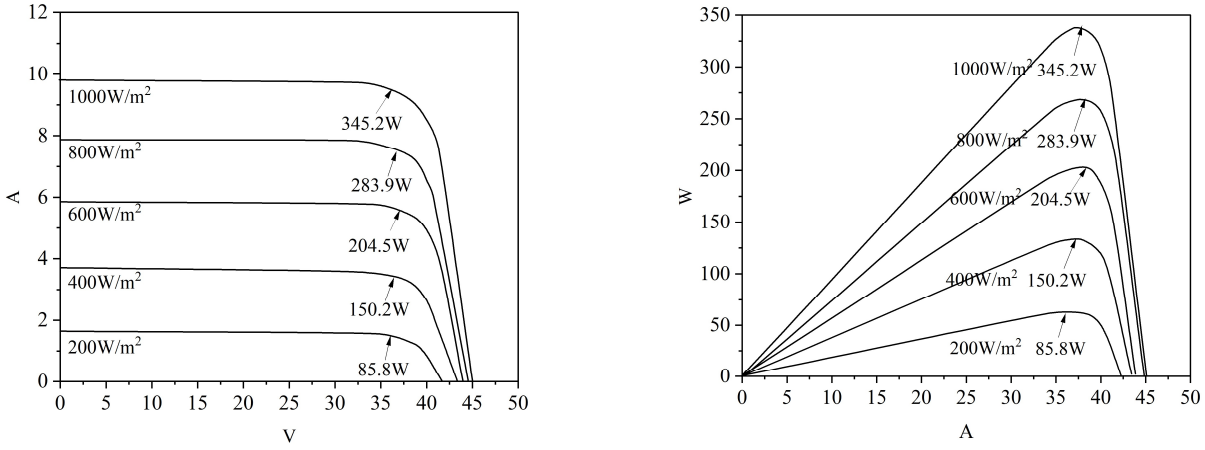

(a) IV curves under different solar illuminance (Battery temperature 20℃)

(b) P-V curves under different solar illuminance (Battery temperature 20℃)

Figure 3: Electrical performance under different irradiation degrees

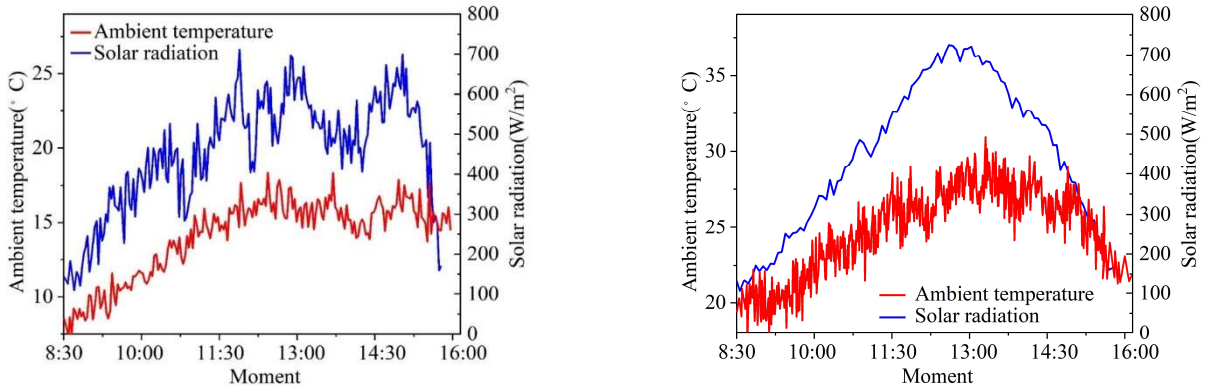

(a) Internal circulation mode

(b) Outer cycle mode

Figure 4: Meteorological data

Figure 5 shows the temperature change trends of system components under external circulation experiments on May 14. The temperature change trends of photovoltaic glass and tempered glass are generally consistent with the irradiation change trends. The maximum temperature of photovoltaic glass is approximately 44°C, while that of tempered glass is approximately 33.5°C. Among these, photovoltaic glass, which directly absorbs solar radiation, exhibits the most significant fluctuations in temperature in response to changes in irradiation. The indoor temperature also followed a trend of first increasing and then decreasing with changes in environmental parameters. Due to the thermal storage and insulation properties of building materials, the magnitude of these changes was the smallest. The air inside the flow channel was heated by the photovoltaic glass, resulting in an average temperature that first increased and then decreased. Since the air inside the flow channel continuously exchanges with the external environment, the temperature measurement results exhibited some fluctuations.

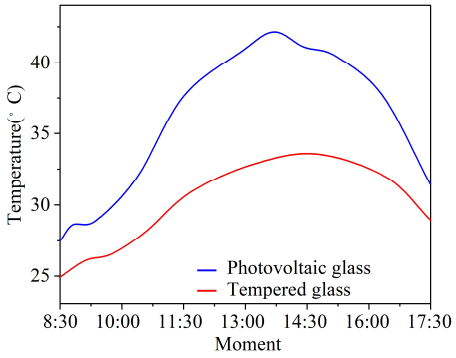

(a) Temperature of photovoltaic glass and tempered glass

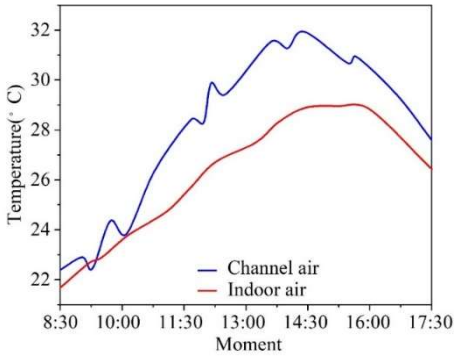

(b) Average temperature of the flow channel and indoor air

Figure 5: The system temperature field in the external circulation mode

Figure 6 shows the temperature change trends of system components under the internal circulation experiment on April 20. Similar to the external circulation, the temperatures of photovoltaic glass and tempered glass fluctuate with changes in irradiation, with photovoltaic glass exhibiting the most significant fluctuations. The maximum temperature of photovoltaic glass is approximately 43°C, while that of tempered glass is approximately 32.5°C. Due to ventilation, the indoor temperature and the air temperature inside the duct show nearly identical temperature changes, with the air temperature inside the duct consistently higher than the indoor air temperature. Therefore, during the experiment, the air duct continuously supplied heat to the indoor space. The maximum temperature rise of the air inside the duct was approximately 17°C, while the maximum temperature rise of the indoor air was approximately 14.5°C. Compared to the external circulation mode, the temperature changes of the air inside the duct were relatively stable. This is because the airflow speed near the thermocouple was slower than that outside, and thus less affected by external wind speeds.

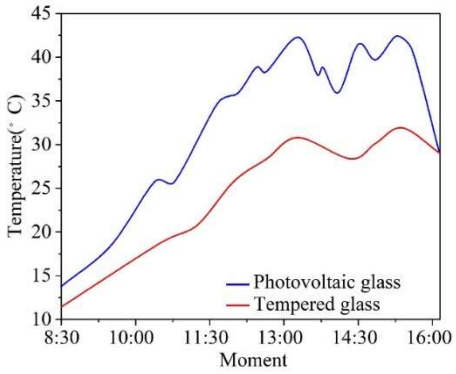

(a) Temperature of photovoltaic glass and tempered glass

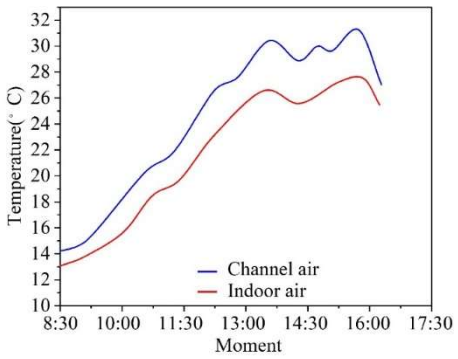

(b) Average temperature of the flow channel and indoor air

Figure 6: The system temperature field in the internal cycle mode

Figure 7 shows the solar heat gain coefficient of copper indium gallium selenide photovoltaic ventilation windows under two operating modes. Since the calculation results have large errors when the irradiance is too low, only the results from 10:00 to 16:00 are retained in the figure. As can be seen from Figure (a), the solar heat gain coefficient varies between 0.15 and 0.5, and the larger the irradiance, the larger the solar heat gain coefficient tends to be. Significant fluctuations occur due to sudden increases or decreases in solar irradiance, as shown in the figure. For example, when irradiance suddenly decreases at a certain moment, the indoor heat gain remains high due to the system's thermal storage, resulting in a sudden increase in the solar heat gain coefficient calculated at that moment. As shown in Figure (b), the solar heat gain coefficient fluctuates around 0.11. Since the irradiance was relatively stable during the experiment, the solar heat gain coefficient changes relatively smoothly. After weighted averaging,

the average solar heat gain coefficient of the system in internal circulation mode is 0.30, and in external circulation mode, it is 0.11.

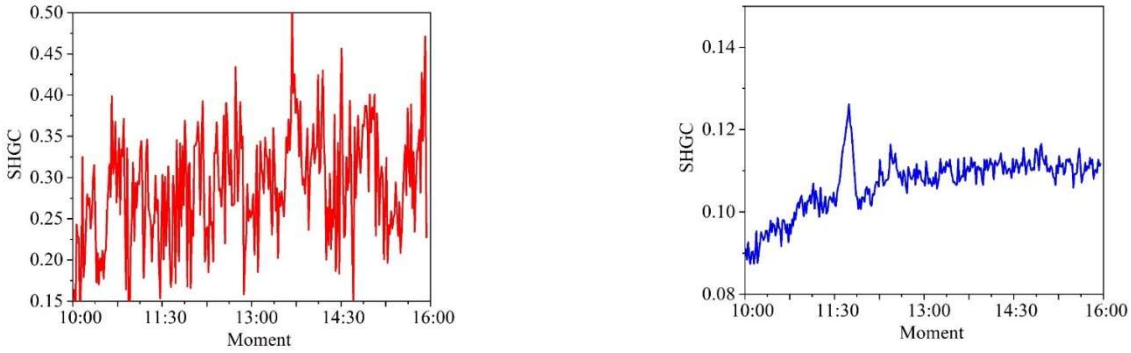

(a) Internal circulation mode (b) External circulation mode

Figure 7: Thermal coefficient of solar power

Figure 8 shows the changes in the thermal insulation coefficient of the copper indium gallium selenide photovoltaic ventilation window under nighttime thermal insulation mode on May 14. Due to the large calculation errors when the indoor-outdoor temperature difference is small, the figure only retains the calculation results from 00:00 to 4:00. As shown in Figure (a), the thermal insulation coefficient fluctuates around 1.8 W/m²·K, with a higher coefficient in the first half of the night and a lower coefficient in the latter half. This is because the outdoor wind speed is higher in the first half of the night, leading to greater heat loss through the window. Figure (b) shows the relationship between heat loss and indoor-outdoor temperature difference during the experiment. It can be seen that heat loss is approximately linearly related to the indoor-outdoor temperature difference, with the slope approximating the average thermal insulation coefficient during the experiment, resulting in 2.09 W/m²·K.

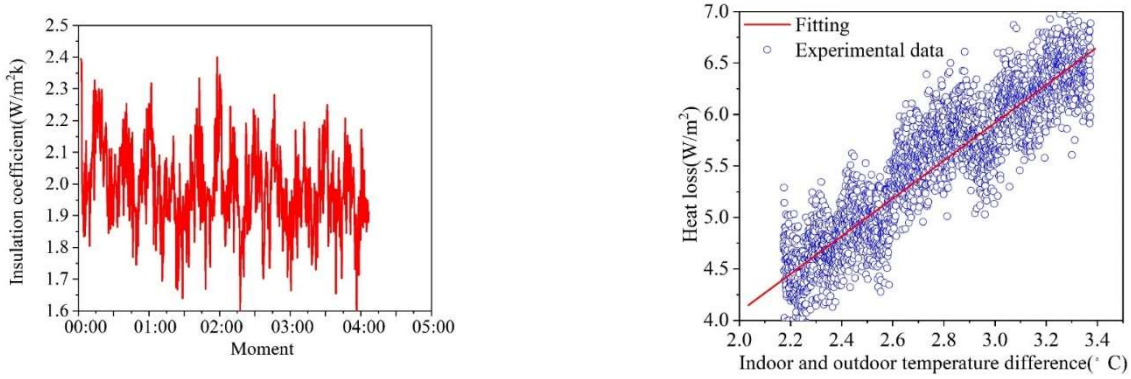

(a) Instantaneous U (b) Mean U value

Figure 8: Insulation coefficient

Figure 9 shows the power generation capacity and photovoltaic conversion efficiency of the copper indium gallium selenide photovoltaic ventilation window under two operating modes. On April 20, under the internal circulation operating mode, the maximum photovoltaic power generation capacity was approximately 162W, with the instantaneous photovoltaic efficiency fluctuating around 7.2%. The total power generation for the day was approximately 0.79kWh, with an average photovoltaic efficiency of 7.0% for the day. In the external cycle operating mode on May 14, the maximum photovoltaic power generation was approximately 122 W, with a total daily power generation of 0.70 kWh and an average daily photovoltaic efficiency of 5.9%. The lower electrical efficiency in the external cycle mode compared to the internal cycle mode is primarily attributed to the higher solar altitude angle on the experimental date, resulting in a larger incident angle of solar radiation on the window surface and higher reflectivity. As shown in the figure, the photovoltaic efficiency exhibits a trend of first decreasing, then increasing, and then decreasing again. The primary reason for this is that in the morning, the south wall primarily receives

diffuse radiation, and the reflectance of diffuse radiation on glass is low, resulting in more radiation reaching the battery surface, thus achieving higher power generation efficiency. By mid-morning, direct radiation appears on the south wall, with a larger incident angle, causing more radiation to be reflected, thereby reducing power generation efficiency. By noon, the angle of incidence of direct solar radiation decreases, reducing reflection and increasing power generation efficiency. In the afternoon, sunlight becomes oblique, increasing the angle of incidence of direct radiation and raising reflection, which again lowers power generation efficiency.

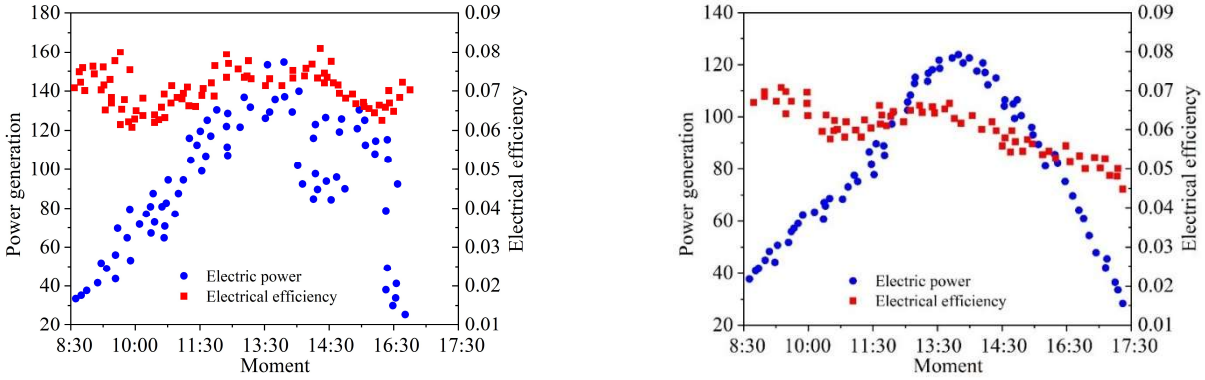

(a) Internal circulation mode

(b) External circulation mode

Figure 9: Power generation capacity and power generation efficiency

Table 5 presents the comparison results of thermal conductivity and power generation performance between copper indium gallium selenide (CIGS) photovoltaic ventilation windows and other photovoltaic windows. Since the SHGC of photovoltaic windows strongly depends on the photovoltaic coverage rate, the values in the table vary significantly, ranging from 0.1 to 0.6. However, the SHGC of other photovoltaic windows is typically a fixed value, while the SHGC of the copper indium gallium selenide photovoltaic ventilation window can be adjusted by switching operating modes to meet different seasonal thermal demands. Compared to photovoltaic double-glazed windows, the copper indium gallium selenide photovoltaic ventilation window has a lower U-value, indicating that the proposed system provides better thermal insulation at night. As shown in the table, photovoltaic vacuum windows and single-layer low-emissivity glass have lower U-values, as vacuum glass has higher thermal resistance, while low-e coatings reflect long-wave infrared radiation back into the room. If the inner glass of the copper indium gallium selenide photovoltaic ventilated window is coated with a low-emissivity film or replaced with vacuum glass, its U-value will further decrease. From the comparison of power generation efficiency, it can be seen that the power generation efficiency of copper indium gallium selenide cells is higher than that of amorphous silicon cells but lower than that of crystalline silicon cells. However, crystalline silicon cells have larger individual sizes, which can severely disrupt the indoor lighting environment.

Table 5: Heat transfer of photovoltaic Windows - comparison of power generation performance

Window type	Region	Photovoltaic efficiency(%)	SHGC	U value(W/m2K)
CIGS photovoltaic ventilation window	Hefei, China	6.2	0.16 external cycle	2.03
Amorphous silicon photovoltaic hollow window	Chengdu, China	4.5	0.22 internal cycle	
Amorphous silicon photovoltaic hollow window	Hong Kong, China	5.2	0.11	/
Amorphous silicon photovoltaic hollow window	Greece, Seferi	/	0.231	2.36
Crystalline silicon photovoltaic hollow window	Chengdu, China	12	0.316	/
Crystalline silicon photovoltaic hollow window	Berkeley, USA	16	0.12	3.56
Amorphous silicon photovoltaic vacuum window	Cornwall, UK	/	0.45	0.85
Amorphous silicon photovoltaic ventilation window	Hong Kong, China	5.46	0.11	3.45
Amorphous silicon photovoltaic blinds	Changsha, China	2.31	0.22	3.36

Amorphous silicon single-layer low-e window	Madrid, Spain	2.88	0.63	1.6
Cadmium telluride single-layer photovoltaic window	Cornwall, UK	6.5	0.22	2.76
Amorphous silicon single-layer photovoltaic window	Singapore	/	0.32	/

V. Daylighting performance of BIPV components

V. A. Ventilation Photovoltaic Window Daylighting Performance

This paper evaluates the daylighting performance of photovoltaic windows using the useful daylighting index (UDI). The useful daylighting index refers to the probability that a point on the indoor reference plane receives illuminance within the useful range from sky diffuse light, either directly or indirectly, during working hours (8:00–18:00), based on the assumed and known sky brightness distribution. The useful range for natural daylighting is between 50 lux and 2,100 lux. Values below 50 lux fall outside the useful range, while values above 2,100 lux exceed the useful range. Within the useful range, when the reference point illuminance is between 50 lux and 450 lux, it indicates that natural daylighting can be used alone or in combination with artificial lighting. When the reference point illuminance is between 450 lux and 2100 lux, it indicates that natural daylighting is satisfactory and within an acceptable range. Figure 10 shows the illuminance levels at the reference points in the ventilated photovoltaic window room. Although the illuminance in the ventilated photovoltaic window room does not meet the office illuminance requirement of 450 lux, it reaches 300 lux at midday, which is sufficient for most indoor activities. The calculated useful daylighting rate for the ventilated photovoltaic window room is 76.43%.

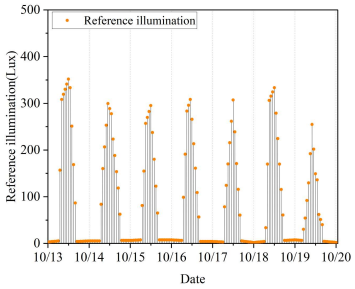

Figure 10: Illumination of ventilation photovoltaic window room

V. B. Comparison of the light transmission performance of photovoltaic windows

Figure 11 compares the daylighting performance of traditional photovoltaic windows and ventilated photovoltaic windows. The daylighting performance comparison is based on the illuminance at specified points within the room. Since office lighting is typically used during workdays, all optical performance comparisons were conducted on holidays. As shown in the figure, the reference point illuminance in rooms with ventilated photovoltaic windows is higher than that in rooms with traditional photovoltaic windows. On a sunny midday, the illuminance at a specified point in a room with ventilated photovoltaic windows can reach 360 lux. Therefore, if this natural light is utilized effectively, adjustable dimming lighting can be used to reduce the room's lighting energy consumption.

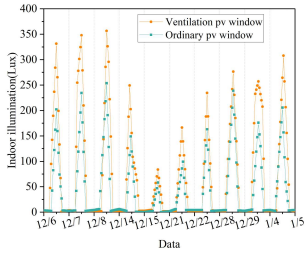

Figure 11: Solar lighting performance comparison of photovoltaic Windows

V. C. Glare Analysis

Glare refers to the phenomenon where overly bright light sources or excessive brightness contrast in the field of view negatively impact visual comfort. To assess the impact of the optimized design proposed in this paper on indoor glare conditions, further comparative analysis was conducted. In the evaluation of indoor lighting

environments in green buildings, the Discomfort Glare Index (DGI) is typically used as an evaluation metric, with the following expression:

$$D_{GI} = 10\lg\sum G_n \tag{2}$$

In the formula: D_{GI} is the discomfort glare index. G_n is the glare constant.

The glare constant can be expressed as:

$$G_n = 0.478\frac{L_s^{1.6}\Omega^{0.8}}{L_b + 0.07\omega^{0.5}L_s} \tag{3}$$

In the formula: L_s is the window brightness, cd/m2. L_b is the background brightness, cd/m^2. ω is the solid angle, sr. Ω is the corrected solid angle, sr.

Among them, the expression for the corrected solid angle is:

$$\Omega = \int\frac{d\omega}{p^2} \tag{4}$$

In the formula: p represents the Guss position index.

Glare calculations were conducted for two scenarios: installing semi-transparent photovoltaic windows made of copper indium gallium selenide (CIGS) and using a traditional photovoltaic window layout. The discomfort glare indices for the areas before and after installing the semi-transparent photovoltaic windows are shown in Figure 12 (Figures A–E represent the southwest facade, southeast facade, northwest facade, southwest facade, and southeast facade, respectively). The figure shows that the overall glare environment of the southwest and southeast facades has improved. On the northwest facade, where translucent photovoltaic windows were not installed, the discomfort glare index increased due to the increased brightness contrast in front of the indoor windows, but it was still below the discomfort glare index limit specified in GB50033-2013 “Building Daylighting Design Standards.”

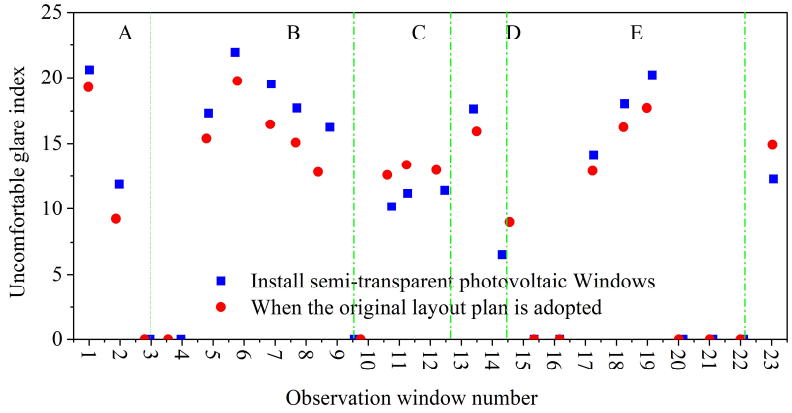

Figure 12: DGI of public office before and after arranging semi-transprent PV windows

VI. Sensitivity analysis of thermoelectric output indicators for BIPV envelope systems

To quantify the sensitivity of each output indicator to changes in each key parameter, the sensitivity index Si is used as a quantitative indicator. The calculation method is shown in the following equation:

$$Si = \frac{\left(PD_{\max} - PD_{\min}\right)}{R_{pc}} \times 100\% \tag{5}$$

In the formula: $PD_{\max}$ —the maximum deviation of the output indicator from the benchmark value, %. $PD_{\min}$ —the minimum deviation of the output indicator from the benchmark value, %. R_{pc} —the range of change of the key parameter from the reference value, %. The physical meaning of the Si value is: the deviation of the system's thermoelectric output indicator from the baseline value under a unit parameter change range. The higher the Si value, the more sensitive the system's thermoelectric output indicator is to changes in that specific parameter, indicating that the parameter is more important to the output indicator.

The sensitivity indices (Si values) of all output indicators for the building envelope systems of representative cities in each climate zone with respect to each key parameter are shown in Table 6. In the table, the sensitivity indices of annual total electricity generation per unit area to changes in air duct spacing, building exterior wall thermal

conductivity coefficient, and photovoltaic curtain wall height are denoted as SdEpv, SUEpv, and SHEpv, respectively. The sensitivity indices of annual total air duct heat generation to changes in air duct spacing, building exterior wall thermal conductivity coefficient, and photovoltaic curtain wall height are denoted as SdQpv, SUQpv, and SHQpv, respectively. The sensitivity indices of annual total indoor heat transfer to changes in air duct spacing, building exterior wall thermal conductivity, and photovoltaic curtain wall height are denoted as SdQroom, SUQroom, and SHQroom, respectively. Overall, the sensitivity indices of annual total electricity generation for typical cities in each climate zone to key parameters are the lowest, with Si ranging from 0% to 2.5%. The sensitivity indices of annual total air duct heat generation and total indoor heat transfer to key parameters are relatively high, with Si variation ranges of 0.4% to 43.2% and 8.8% to 87.6%, respectively.

Table 6: Thermoelectric output indicators are sensitive to key parameters (%)

Sensitivity factor	SdEpv	SUEpv	SHEpv	SdQpv	SUQpv	SHQpv	SdQroom	SUQroom	SHQroom
Harbin	1.1	0	0.4	43.2	0.6	8.5	36.2	25.3	10.2
Urumqi	1.5	0	0.2	40.21	0.4	8.6	30.6	32.2	8.8
Guangzhou	2.5	0	0.6	39.6	1.7	8.2	21.3	76.3	10.2
Kunming	1.9	0	0.3	38.6	2.5	8.2	41.6	87.6	14.6

The annual total electricity generation per unit area of representative cities in each climate zone is most sensitive to changes in air duct spacing, with a sensitivity index (SdEpv) of 1.1% to 2.5%. Next is the height of photovoltaic curtain walls, with a sensitivity index (SHEpv) of 0.2% to 0.6%. Changes in the thermal conductivity coefficient of building facades have little effect. The primary reason is that the system's annual total electricity generation is primarily determined by instantaneous power generation efficiency. As indicated by the aforementioned experimental studies, changes in the natural convection intensity of air ducts directly result in changes in backplate temperature and airflow velocity, which directly impact the system's instantaneous power generation capacity. Among these factors, air duct spacing has the greatest influence on natural convection within the ducts, followed by photovoltaic curtain wall height.

The annual total heat generation per unit area of air ducts in representative cities across different climate zones is also most sensitive to changes in air duct spacing, with a sensitivity index SdQpv ranging from 38.6% to 43.2%. Next is the height of the photovoltaic curtain wall, with a sensitivity index SHQpv ranging from 8.2% to 8.6%, followed by the thermal conductivity coefficient of the building exterior wall, with a sensitivity index SUQpv ranging from 0.4% to 2.5%. The reason for this is that the heat generated by air ducts is primarily determined by the outlet temperature of the ducts and the average airflow velocity, both of which depend on the natural convection effect of the air ducts. As mentioned earlier, the spacing between air ducts and the height of photovoltaic curtain walls are the primary parameters affecting the natural convection effect.

The annual total indoor heat transfer per unit area in representative cities across different climate zones is sensitive to changes in all key parameters. In the Harbin region, the annual total indoor heat transfer is most sensitive to changes in air duct spacing, with a sensitivity index (SdQroom) of 36.2%, followed by the building exterior wall heat transfer coefficient, with a sensitivity index (SUQroom) of 25.3%. In other climate zones, the annual total indoor heat transfer is most sensitive to changes in the building exterior wall heat transfer coefficient, followed by air duct spacing.

VII. Optimization Design Strategy for BIPV Perimeter Protection Systems

VII. A. BIPV tilt angle design and installation

In practical applications, the installation area of photovoltaic modules is closely related to the total power generation. When arranging the modules, the primary consideration should be the impact of shadowing. As seasons change, the installation angle and spacing of photovoltaic modules should be adjusted to mitigate this effect. According to “GB50797-2012 Photovoltaic Power Station Design Code,” the layout of photovoltaic arrays should ensure that there is no shadow blocking between 9:00 and 15:00 (true solar time) every day in order to find the optimal installation angle for photovoltaic modules on buildings.

Using PVsyst software, analyze the shadows cast by photovoltaic modules on facades and roofs during different seasons. The simulation location is Harbin, Heilongjiang Province (126.8°E, 45.8°N), with photovoltaic panels 1m wide, bottom and top frames of the light-receiving surface both 0.03m, and an array of 5 rows. The simulation assumes that the width of the building roof and the height of the facade are both 12m, allowing sufficient space for adjusting the spacing and angle of the photovoltaic modules.

VII. A. 1) Building Roofs

Installing photovoltaic modules on rooftops can significantly reduce environmental shading. When installing photovoltaic modules on flat roofs, the primary consideration is the maximum solar radiation acceptance angle for the region throughout the year. Additionally, differences in solar altitude angles across seasons result in variations in the planar utilization coefficient of rooftop modules. An analysis of rooftop shading factors is shown in Table 7.

Table 7: Analysis of influence factors of roof shadow

	Height of sun(°)	Photoelectric conversion maximum dip(°)	The spacing of the photovoltaic panels (m)	Utilization coefficient	Shadow threshold(°)
Equinox	29.46-44.12	45.75	1.91	0.64	29.43
Summer solstice	47.5-68.07	22.3	1.24	0.73	46.74
Autumn equinox	29.6-44.25	46.15	1.99	0.49	29.31
Winter solstice	9.41-20.73	69.24	5.5	0.11	9.62

The plane utilization coefficient = lighting surface area / inter-row roof area. The shadow critical angle should be slightly smaller than the solar altitude angle to ensure that photovoltaic modules are not shaded while maximizing plane utilization efficiency.

As shown in the table, there is no difference in the data between the vernal equinox and the autumnal equinox, as these two periods have the same latitude angle. The spacing between photovoltaic panels is smallest at the summer solstice and largest at the winter solstice, which is related to the range of changes in the solar altitude angle. The higher the shadow critical angle, the smaller the spacing between photovoltaic panels. Conversely, the lower the shadow critical angle, the larger the spacing between photovoltaic panels.

Since the total duration of sunlight in spring and autumn accounts for the largest proportion, the optimal installation angle for flat roofs should be based on the shadow critical angle at the spring (or autumn) equinox, with other angle utilization coefficients and economic indicators compared and balanced accordingly.

For sloped roofs, the installation angle of the modules is typically equal to the roof design slope, eliminating issues of module shading. In this case, the roof design slope should be selected based on the angle corresponding to the maximum annual radiation in the region for optimal performance.

VII. A. 2) Building Facades

The installation angle of photovoltaic modules has a significant impact on the aesthetic appeal of building facades. However, in extremely cold, high-latitude regions with low solar elevation angles, installing photovoltaic modules with larger tilt angles on building facades can more effectively maximize their performance. When simulating vertical facades, unlike building roofs, there is no need to consider utilization coefficients. However, the shadow critical angle should be slightly greater than the solar elevation angle range to ensure that photovoltaic modules do not cast shadows on one another. With parameters and selected conditions unchanged, the analysis of shadow influence factors on south-facing facades is shown in Table 8.

Table 8: Analysis of the influence factors of the southern façade

	Height of sun(°)	Photoelectric conversion maximum dip(°)	The spacing of the photovoltaic panels (m)	Shadow threshold(°)
Equinox	29.46-44.12	45.75	1.25	44.43
Summer solstice	47.5-68.07	22.3	2.6	67.85
Autumn equinox	29.6-44.25	46.15	1.42	44.68
Winter solstice	9.41-20.73	69.24	1.16	21.95

VII. B. BIPV Design Strategies

VII. B. 1) Roof Design Strategies

Building roofs offer greater flexibility in terms of spacing and tilt angles for photovoltaic (PV) modules, while also enhancing their conversion efficiency. In practical applications, the size of the installation site must also be considered. The installed area of PV modules remains constant throughout the year, with spring and autumn installation areas serving as the standard. This section selects a site with a width of 12 meters, using Harbin as an

example, to simulate the radiation intensity received by photovoltaic modules in different seasons. The simulation results for building roof angle designs from spring to winter are shown in Tables 9–12. The annual building roof angle design is shown in Table 13.

The economic benefits in the table are the ratio of the total radiation received per unit area of photovoltaic panels to the price per square meter of photovoltaic modules. Based on the analysis of the above tables: When the site area is limited, the installation area of photovoltaic modules is determined by the installation angle, number of modules, and installation spacing. The smaller the installation angle of the photovoltaic panels, the smaller the spacing between them, resulting in more photovoltaic modules that can be installed and a larger installation area. The total radiation received is directly related to the power generation capacity; the more radiation received, the higher the power generation capacity. In spring, summer, autumn, and winter, the angle at which photovoltaic panels receive the highest total radiation is 10°, but the economic benefit is the lowest. When the installation angle of photovoltaic modules is 40°, the annual economic benefit is the highest, at 4.16. At this point, the installation area of photovoltaic modules is 8.72 m², and the installation spacing is 1.8 m, which meets the acceptability of photovoltaic modules from an architect's perspective.

Table 9: Design of roof angles for buildings in spring

Installation spacing(m)	Shadow critical Angle(°)	Installation Angle(°)	Installation area(m2)	The total amount of radiation received by photovoltaic panels in spring (KWh/m^2)	Economic benefits
1.91	29.6	45	8.44	580.18	0.99
1.8	29.6	40	8.72	595	0.99
1.65	29.2	30	9.38	628.9	0.94
1.24	29.5	20	10.7	687.54	0.9
1.11	29.4	10	12.89	775.76	0.86

Table 10: Design of roof Angle of summer building

Installation spacing(m)	Shadow critical Angle(°)	Installation Angle(°)	Installation area(m^2)	The total amount of radiation received by photovoltaic panels (KWh/m^2)	Economic benefits
1.91	29.6	45	8.44	729.96	1.24
1.8	29.6	40	8.72	778.46	1.28
1.65	29.2	30	9.38	857.32	1.26
1.24	29.5	20	10.7	980.29	1.37
1.11	29.4	10	12.89	1151.26	1.24

Table 11: Design of roof Angle of autumn building

Installation spacing(m)	Shadow critical Angle(°)	Installation Angle(°)	Installation area(m^2)	The total amount of radiation received by photovoltaic panels (KWh/m^2)	Economic benefits
1.91	29.6	45	8.44	627.7	1.08
1.8	29.6	40	8.72	643.15	1.01
1.65	29.2	30	9.38	683.98	1.07
1.24	29.5	20	10.7	761.14	1.08
1.11	29.4	10	12.89	858.69	0.97

Table 12: Roof Angle design for buildings in winter

Installation spacing(m)	Shadow critical Angle(°)	Installation Angle(°)	Installation area(m^2)	The total amount of radiation received by photovoltaic panels (KWh/m^2)	Economic benefits
1.91	29.6	45	8.44	414.63	0.66
1.8	29.6	40	8.72	417.84	0.68
1.65	29.2	30	9.38	429.98	0.63
1.24	29.5	20	10.7	461.42	0.56
1.11	29.4	10	12.89	512.67	0.59

Table 13: Roof Angle design for buildings throughout the year

Installation spacing(m)	Installation Angle (°)	Installation area (m^2)	The total amount of radiation received by photovoltaic panels (KWh/m^2)	Economic benefits
1.91	45	8.44	2352.47	3.97
1.8	40	8.72	2434.45	4.16
1.65	30	9.38	2600.18	3.9
1.24	20	10.7	2890.39	3.91
1.11	10	12.89	3298.38	3.66

VII. B. 2) Facade Design Strategy

Like building roofs, photovoltaic modules installed on building facades maintain a constant installation area throughout the year, with spring and autumn installation areas serving as the standard. A site with a height of 12 meters was selected to simulate the installation area of photovoltaic modules on building facades, with the solar altitude angle slightly less than the shadow critical angle. The simulation results for the design angles of building facades from spring to winter are shown in Tables 14 to 17. The annual design angles for building facades are shown in Table 18.

Similar to building roofs, the more photovoltaic modules are installed, the more radiation resources are received, but the economic benefits are the lowest. In the Harbin region, the economic benefit is lowest when photovoltaic modules are installed at an angle of 80° on the building facade. The highest annual economic benefit of 4.44 is achieved when the installation angle is 45°, with an installation area of 14.96 m² and an installation spacing of 1 m. Photovoltaic modules installed at a 45° angle on the building facade also meet the acceptability criteria from an architectural perspective.

Table 14: Design of the architectural facade of spring

Installation spacing(m)	Shadow critical Angle(°)	Installation Angle(°)	Installation area (m^2)	The total amount of radiation received by photovoltaic panels (KWh/m^2)	Economic benefits
1	28.2	45	14.96	1022.7	1.17
1.04	30.9	50	14.45	994.36	0.88
1.01	30.8	60	14.48	973.22	0.66
1.05	29.5	70	14.33	953.32	0.87
1	29.8	80	15.09	950.62	0.82

Table 15: Design of the architectural facade of summer

Installation spacing(m)	Shadow critical Angle(°)	Installation Angle(°)	Installation area (m^2)	The total amount of radiation received by photovoltaic panels (KWh/m^2)	Economic benefits
1	28.2	45	14.96	1307	1.16
1.04	30.9	50	14.45	1239.14	1.04
1.01	30.8	60	14.48	1148.34	1.17
1.05	29.5	70	14.33	1057.01	1.15
1	29.8	80	15.09	990.07	0.88

Table 16: Design of the architectural facade of autumn

Installation spacing(m)	Shadow critical Angle(°)	Installation Angle(°)	Installation area (m^2)	The total amount of radiation received by photovoltaic panels (KWh/m^2)	Economic benefits
1	28.2	45	14.96	1109.33	1.29
1.04	30.9	50	14.45	1075.36	0.93
1.01	30.8	60	14.48	1043.03	1.04
1.05	29.5	70	14.33	1010.72	1.03
1	29.8	80	15.09	1001.99	0.78

Table 17: Design of the architectural facade of winter

Installation spacing(m)	Shadow critical Angle(°)	Installation Angle(°)	Installation area (m^2)	The total amount of radiation received by photovoltaic panels (KWh/m^2)	Economic benefits
1	28.2	45	14.96	730.76	0.82
1.04	30.9	50	14.45	719.44	0.76
1.01	30.8	60	14.48	726.14	0.59
1.05	29.5	70	14.33	742.79	0.71
1	29.8	80	15.09	776.27	0.73

Table 18: The design of building facade angles throughout the year in Harbin

Installation spacing(m)	Installation Angle(°)	Installation area (m^2)	The total amount of radiation received by photovoltaic panels (KWh/m^2)	Economic benefits
1	45	14.96	4169.79	4.44
1.04	50	14.45	4028.3	3.61
1.01	60	14.48	3890.73	3.46
1.05	70	14.33	3763.84	3.76
1	80	15.09	3718.95	3.21

VIII. Conclusion

As society develops and the demand for improved living standards grows, the proportion of building energy consumption in total societal energy consumption continues to rise. Since building envelopes have a significant impact on building energy consumption, it is necessary to conduct research on building envelopes. To this end, this paper designs a new BIPV exterior envelope system. The copper indium gallium selenide (CIGS) photovoltaic ventilation windows offer better thermal insulation and have a lower U-value compared to photovoltaic double-glazed windows. Their power generation efficiency is higher than that of amorphous silicon cells but lower than that of crystalline silicon cells. However, crystalline silicon cells have poor light transmission performance. In October, the effective light transmission rate of the photovoltaic windows reached 76.43%, with room illuminance reaching 300 lux, sufficient to support most indoor activities. According to sensitivity analysis results, the sensitivity index of annual total power generation for typical cities in various climate zones to key parameters is the lowest, with Si values ranging from 0% to 2.5%. The annual total airflow heat generation and total indoor heat transfer have relatively high sensitivity indices for key parameters, with Si values ranging from (0.4% to 43.2%) and (8.8% to 87.6%), respectively.

Finally, a comprehensive analysis was conducted on the design and installation angles of photovoltaic modules. The installation angle of photovoltaic modules on the building roof is 40°, with an installation area of 8.72 m² and an installation spacing of 1.8 m, yielding the highest economic benefit (4.16). For photovoltaic modules on the building facade, an installation angle of 45°, an installation area of 14.96 m², and an installation spacing of 1 m result in the highest annual economic benefit of 4.44.

Funding

This work was supported by CSCEC Project: Research and Development and Application Demonstration of New Building-Integrated Photovoltaics Envelope (CSCEC-2023-Z-3).

References

[1] Ahmed, M. (2016). Greenhouse gas emissions and climate variability: An overview. Quantification of climate variability, adaptation and mitigation for agricultural sustainability, 1-26.

[2] Erickson, L. E. (2017). Reducing greenhouse gas emissions and improving air quality: Two global challenges. Environmental progress & sustainable energy, 36(4), 982-988.

[3] Cassia, R., Nocioni, M., Correa-Aragunde, N., & Lamattina, L. (2018). Climate change and the impact of greenhouse gasses: CO2 and NO, friends and foes of plant oxidative stress. Frontiers in plant science, 9, 273.

[4] Lugo-Morin, D. R. (2021). Global future: low-carbon economy or high-carbon economy?. World, 2(2), 175-193.

[5] Yang, W., Zhao, R., Chuai, X., Xiao, L., Cao, L., Zhang, Z., ... & Yao, L. (2019). China's pathway to a low carbon economy. Carbon balance and management, 14, 1-12.

[6] Gao, M. (2023). The impacts of carbon trading policy on China's low-carbon economy based on county-level perspectives. Energy Policy, 175, 113494.

[7] Bridge, G., Bouzarovski, S., Bradshaw, M., & Eyre, N. (2013). Geographies of energy transition: Space, place and the low-carbon economy. Energy policy, 53, 331-340.

[8] Tavoni, M., De Cian, E., Luderer, G., Steckel, J. C., & Waisman, H. (2012). The value of technology and of its evolution towards a low carbon economy. Climatic Change, 114, 39-57.
[9] Chen, T., An, Y., & Heng, C. K. (2022). A review of building-integrated photovoltaics in Singapore: Status, barriers, and prospects. Sustainability, 14(16), 10160.
[10] Shakouri, M., Ghadamian, H., Hoseinzadeh, S., & Sohani, A. (2022). Multi-objective 4E analysis for a building integrated photovoltaic thermal double skin Façade system. Solar Energy, 233, 408-420.
[11] Zhang, T., Wang, M., & Yang, H. (2018). A review of the energy performance and life-cycle assessment of building-integrated photovoltaic (BIPV) systems. Energies, 11(11), 3157.
[12] Dehwah, A. H., & Krarti, M. (2021). Energy performance of integrated adaptive envelope systems for residential buildings. Energy, 233, 121165.
[13] Choi, W. J., Joo, H. J., Park, J. W., Kim, S. K., & Lee, J. B. (2019). Power generation performance of building-integrated photovoltaic systems in a Zero Energy Building. Energies, 12(13), 2471.
[14] Gagliano, A., Tina, G. M., Aneli, S., & Chemisana, D. (2021). Analysis of the performances of a building-integrated PV/Thermal system. Journal of Cleaner Production, 320, 128876.
[15] Saadon, S., Gaillard, L., Giroux-Julien, S., & Ménézo, C. (2016). Simulation study of a naturally-ventilated building integrated photovoltaic/thermal (BIPV/T) envelope. Renewable Energy, 87, 517-531.
[16] Youssef, A. M., Zhai, Z. J., & Reffat, R. M. (2015, June). Design of optimal building envelopes with integrated photovoltaics. In Building Simulation (Vol. 8, pp. 353-366). Tsinghua University Press.
[17] Samarasinghalage, T. I., Wijeratne, W. P. U., Yang, R. J., & Wakefield, R. (2022). A multi-objective optimization framework for building-integrated PV envelope design balancing energy and cost. Journal of Cleaner Production, 342, 130930.
[18] Saadon, S., Gaillard, L., Giroux, S., & Ménézo, C. (2015). Simulation study of a naturally ventilated building integrated photovoltaic (BIPV) envelope. Energy Procedia, 78, 2004-2009.
[19] Yin, H. M., Yang, D. J., Kelly, G., & Garant, J. (2013). Design and performance of a novel building integrated PV/thermal system for energy efficiency of buildings. Solar Energy, 87, 184-195.
[20] Asefi, G., Habibollahzade, A., Ma, T., Houshfar, E., & Wang, R. (2021). Thermal management of building-integrated photovoltaic/thermal systems: A comprehensive review. Solar Energy, 216, 188-210.
[21] Mosalam, H. (2018, December). Evaluation Study Design and Operation of a Building Integrated Photovoltaic System. In 2018 International Conference on Smart Grid (icSmartGrid) (pp. 195-201). IEEE.
[22] Wang, Y., Ke, S., Liu, F., Li, J., & Pei, G. (2017). Performance of a building-integrated photovoltaic/thermal system under frame shadows. Energy and Buildings, 134, 71-79.
[23] Maestro, S., Chemisana, D., & Lamnatou, C. (2025). Optics for smart building-integrated photovoltaic systems. Renewable Energy, 122850.
[24] Luo, Y., Cheng, N., Zhang, S., Tian, Z., Xu, G., Yang, X., & Fan, J. (2022, November). Comprehensive energy, economic, environmental assessment of a building integrated photovoltaic-thermoelectric system with battery storage for net zero energy building. In Building Simulation (Vol. 15, No. 11, pp. 1923-1941). Beijing: Tsinghua University Press.
[25] Ravyts, S., Dalla Vecchia, M., Van den Broeck, G., & Driesen, J. (2019). Review on building-integrated photovoltaics electrical system requirements and module-integrated converter recommendations. Energies, 12(8), 1532.
[26] Gupta, N., & Tiwari, G. N. (2017). Energy matrices of building integrated photovoltaic thermal systems: case study. Journal of Architectural Engineering, 23(4), 05017006.
[27] Farghaly, Y., & Hassan, F. (2019). A simulated study of building integrated photovoltaics (BIPV) as an approach for energy retrofit in buildings. Energies, 12(20), 3946.
[28] Shukla, A. K., Sudhakar, K., & Baredar, P. (2016). A comprehensive review on design of building integrated photovoltaic system. Energy and Buildings, 128, 99-110.
[29] Azami, A., & Sevinç, H. (2021). The energy performance of building integrated photovoltaics (BIPV) by determination of optimal building envelope. Building and environment, 199, 107856.
[30] Agathokleous, R. A., & Kalogirou, S. A. (2020). Status, barriers and perspectives of building integrated photovoltaic systems. Energy, 191, 116471.
[31] Şirin, C., Goggins, J., & Hajdukiewicz, M. (2023). A review on building-integrated photovoltaic/thermal systems for green buildings. Applied Thermal Engineering, 229, 120607.
[32] Shankar, A., Vijayakumar, K., & Chitti Babu, B. (2021). Techno-economic and energy assessment of building integrated photovoltaic module as an envelope of the building. International Transactions on Electrical Energy Systems, 31(11), e13105.
[33] Faes, A., Virtuani, A., Quest, H., Maturi, L., Scognamiglio, A., Frontini, F., ... & Ballif, C. (2025). Building-integrated photovoltaics. Nature Reviews Clean Technology, 1-18.
[34] Gholami, H., Røstvik, H. N., & Müller-Eie, D. (2019). Holistic economic analysis of building integrated photovoltaics (BIPV) system: Case studies evaluation. Energy and Buildings, 203, 109461.
[35] Yang, T., & Athienitis, A. K. (2016). A review of research and developments of building-integrated photovoltaic/thermal (BIPV/T) systems. Renewable and Sustainable Energy Reviews, 66, 886-912.
[36] Ramanan, P., Kalidasa Murugavel, K., Karthick, A., & Sudhakar, K. (2020). Performance evaluation of building-integrated photovoltaic systems for residential buildings in southern India. Building Services Engineering Research and Technology, 41(4), 492-506.
[37] Kong, J., Dong, Y., Poshnath, A., Rismanchi, B., & Yap, P. S. (2023). Application of building integrated photovoltaic (BIPV) in net-zero energy buildings (NZEBs). Energies, 16(17), 6401.
[38] Ou, W. S. (2015). Development of Novel Building-Integrated Photovoltaic (BIPV) System in Building Architectural Envelope. In Solar Radiation Applications. IntechOpen.
[39] Martín-Chivelet, N., Kapsis, K., Wilson, H. R., Delisle, V., Yang, R., Olivieri, L., ... & Wijeratne, W. P. U. (2022). Building-Integrated Photovoltaic (BIPV) products and systems: A review of energy-related behavior. Energy and Buildings, 262, 111998.
[40] Aguacil, S., Duque, S., Lufkin, S., & Rey, E. (2024). Designing with building-integrated photovoltaics (BIPV): A pathway to decarbonize residential buildings. Journal of Building Engineering, 96, 110486.
[41] Yuxin Bao & Changying Xiang. (2025). Energy performance and aesthetic perception of colored building-integrated photovoltaic application – A case study in Hong Kong. Energy & Buildings,344,116038-116038.